Paper No.
04379

CORROSION2004

ELECTROCHEMICAL INVESTIGATION AND MODELING OF CARBON DIOXIDE CORROSION OF CARBON STEEL IN THE PRESENCE OF ACETIC ACID

Keith George and Srdjan Nesic
Institute for Corrosion and Multiphase Technology
Ohio University, Athens, OH 45701

Cornelis de Waard
Corrosion Consultancy
Generaal Winkelmanlaan 77
211 WV Aerdenhout, Netherlands

ABSTRACT

Weight loss (WL) and linear polarization resistance (LPR) measurements have been used to verify the effect of acetic acid (HAc) on the anodic and cathodic reactions in CO_2 corrosion of carbon steel. The experiments were performed using a standard rotating cylinder three-electrode system, in a 3% NaCl solution, in a temperature range of 22-60°C and at pH 4. The HAc concentration range used in the study was 0-1000 ppm. An electrochemical model has also been developed to predict the experimental potentiodynamic sweeps and corrosion rates which were compared with the weight loss and LPR measurements. In another modeling development, an additional term has been added to the latest de Waard corrosion model to account for HAc. The modified de Waard model was also compared to the experimental measurements.

Key words: acetic acid, potentiodynamic sweeps, rotating cylinder, electrochemical modeling.

INTRODUCTION

When a gaseous phase of HAc is present in multiphase pipelines it, in addition to carbon dioxide, dissolves into the aqueous solution. The HAc then dissociates into hydrogen and acetate ions

$$HAc \Leftrightarrow H^+ + Ac^- \quad (1)$$

Since HAc is a stronger acid than carbonic acid (pKa 4.76 vs 6.35 at 25°C), it is the main source of hydrogen ions when the two acid concentrations are similar. The acetate ions form iron acetate upon reaction with iron

$$Fe + 2HAc \Rightarrow Fe(Ac)_2 + H_2 \quad (2)$$

But, iron acetate's solubility is much higher than iron carbonate's, so protective film formation by iron acetate does not readily occur. Without formation of a stable protective film, the corrosion rates of the steel can remain at a high value.

Some understanding of the role of HAc in CO_2 corrosion comes from field experience as related to the so-called Top-of-Line-Corrosion (Gunaltun 2000). But, very few systematic studies have been performed in the laboratory. Little or no information exists about the basic effect of HAc on the anodic and cathodic reactions. Hedges and McVeigh (1999) reported a mild increase in the cathodic reaction in the presence of HAc although their results were not fully conclusive. The work of Crolet et al. (1999) suggests that the presence of HAc inhibits the anodic (iron dissolution) reaction.

Crolet et al. (1999) were of some of the first to report on low concentrations of HAc (6-60 ppm) affecting the corrosion rates of carbon steel. They argue that the increase in the rate of corrosion in the presence of HAc occurs due to an inversion in the bicarbonate/acetate ratio. At this inversion point, HAc is the predominant acid compared to carbonic acid and is therefore the main source of acidity.

Hedges and McVeigh (1999) published results on acetate's role in CO_2 corrosion. Experiments using both HAc and sodium acetate as a source of acetate ions in various media (3% NaCl and two synthetic oilfield brines) were performed using rotating cylinder electrodes. Both sources of acetate ions were shown to increase the corrosion rate, while acetic acid decreased the pH while sodium acetate increased it. The increased corrosion rates were attributed to the forming of thinner iron carbonate films since acetate ions have the ability to form iron acetate and transport iron away from the steel surface. However, no attempt was made to quantify the thickness or morphology of the films formed in their experiments.

Garsany et al. (2002) published work using voltammetry to study the effect of acetate ions on the rates and mechanisms of corrosion using a rotating disc electrode (RDE) on film-free surfaces. Their voltammograms show two waves, which are attributed to hydrogen ion and HAc reduction on the steel surface. They argue that since HAc dissociation can occur very quickly it is not possible to distinguish the reduction of hydrogen ions from direct HAc reduction at the electrode surface.

Sun et al. (2003) recently published work using potentiodynamic sweeps to the study the effect of HAc on the cathodic and anodic reactions using a rotating cylinder electrode (RCE). Their work suggests HAc acts solely as an additional source of hydrogen ions and is not reduced at the surface.

EXPERIMENTAL

A schematic of the experimental cell is shown in Figure 1. To begin, the experimental apparatus was assembled, a salt solution was prepared, added to the cell, and then de-oxygenated for one hour using carbon dioxide gas. The test temperature was set using a hot plate and controlled using a feedback temperature probe. Once de-oxygenation had occurred and the test temperature was reached, the appropriate amount of HAc was then added to the cell and de-oxygenation continued for an additional 30 minutes. Since HAc is volatile and the bubbling CO_2 gas could strip the HAc out of the test cell, a

preconditioning cell was used. The preconditioning cell was kept constant at the test temperature and contained the same fluid composition as the experimental cell. The preconditioning cell ensured the CO_2 entering the experimental cell was saturated with HAc and H_2O vapor.

The pH meter used in the experiments was calibrated at the test temperature by heating of the buffer solutions. The pH was monitored before and after the HAc addition to ensure the fluid composition was similar between test runs. In order to achieve the desired system pH, minute adjustments were made using droplets of hydrochloric acid and sodium bicarbonate solutions. The electrode was then immersed into the test solution and the electrode's rotational velocity was set. After approximately 30 additional minutes, electrical connections were made and measurements started.

All electrochemical measurements were made using a potentiostat. The potentiodynamic sweeps were conducted at a sweep rate of 0.2 mV/s and the solution resistance was manually corrected after measurement using electrochemical impedance spectroscopy (EIS). The potentiodynamic sweeps were always conducted starting from the corrosion potential. All measurements were made using a reference electrode. Potentiodynamic sweeps were conducted at constant pH with the pH adjustment occurring after each sweep. Anodic sweeps were limited to polarization less than 200 mV above the corrosion potential to limit excessive iron concentrations in the test cell. The LPR measurements were taken at ±5 mV around the corrosion potential.

The electrode was machined from the parent steel material and had a diameter of 1.20 cm and an area of 5.4 cm^2. The composition of the X-65 mild steel (as reported by the manufacturer) used in the experiments is shown in Table 1. The test matrix for the experimental work is shown in Table 2.

Weight loss Experiments

After the solution had come to the desired temperature and the pH was adjusted, a pre-weighed electrode was immersed into the solution. During the twenty-four hour weight loss experiments, the pH was adjusted approximately every hour or two, which corresponded with LPR measurements. After twenty-four hours, the coupon were taken out of the test solution, rinsed with alcohol, wiped with a soft cloth to remove any corrosion product, and then weighed after drying.

RESULTS AND DISCUSSION

A series of weight loss experiments was initiated to verify the effect of temperature and HAc on the corrosion of mild steel in 3% sodium chloride solutions and the results are shown in Figures 2-4. The average value is presented and the error bars represent the maximum and minimum values. The number above the error bars represents the number of experiments used to calculate the average value. This format will be repeated in the following charts. The values presented for the LPR method are time-averaged over the course of the experiment. Some weight loss experiments were performed using no electrochemistry to see if, by measuring the corrosion rate using LPR, the system was disturbed enough to change the corrosion rate measured by weight loss. Electrochemistry, by LPR, was not found to affect the corrosion rates measured by weight loss.

The effect of increasing temperature on the corrosion rate in solutions containing 0 ppm and 100 ppm HAc measured in 3% sodium chloride solutions is shown in Figure 2. It is evident that the corrosion rates measured using LPR and by weight loss are not in perfect agreement, even when HAc is not present. The B value used to convert the polarization resistances to corrosion currents was calculated using Tafel slopes calculated from Eqn 6. At room temperature, symmetry factors (α) were

used such that b_a=40 mV/dec when no HAc was present and b_c=120 mV/dec. When HAc was present b_a was found to be 80 mV/dec at room temperature (Sun 2003). As the temperature increases, the influence of HAc is more pronounced. For example, at 22°C, adding 100 ppm HAc increases the corrosion rate approximately 30%, while at 60°C the same increase in HAc concentration doubles the corrosion rate.

The effect of adding HAc to 3% sodium chloride solutions at pH of 4 and at 60°C is shown in Figure 3. It is evident that even a 10 ppm HAc addition to the solution affects the corrosion rate. An increase in the HAc concentration to 1000 ppm is shown in Figure 4. It is worth noting that the 1000 ppm HAc, 24-hour weight loss experiment was performed four times. In two of the tests, weight loss measurements on the order of approximately 45 mm/yr were observed and these results are presented in Figure 4. In the other two experiments, the samples experienced pitting corrosion. No discernable difference between the four experiments could be found to identify the trigger for the pitting corrosion.

Experiments in a Simulated Brine Solution

Potentiodynamic sweeps were performed in a simulated brine and compared to 3% sodium chloride solutions containing 100 ppm HAc at pH 4, to study the effect of the presence of multiple ions (Ca^{2+}, Mg^{2+}, Sr^{2+}, K^{+}, HCO_3^{-}) on the electrochemical reactions. The chemical components of the simulated brine solution are given in Table 3. The 3% NaCl potentiodynamic sweeps have been reported elsewhere (Sun et al. 2003) and only the data will be shown here. The potentiodynamic sweeps for the two solutions is shown in Figure 5. It is evident that no difference is apparent for the anodic reaction. There is a change in the cathodic reaction; however, and this is probably due to scaling of the electrode due to the pH increase during the potentiodynamic sweep.

A comparison between the weight loss and LPR measurements was made between solutions containing only 3% sodium chloride and the simulated brine solutions containing 100 ppm HAc at pH 4. The results are shown in Figure 6 and no significant difference can be seen from the weight loss measurements, measured over twenty-four hours between the two solutions.

ELECTROCHEMICAL MODEL

In order to model the experimental results, the nature of the measured cathodic and anodic reactions must be found. HAc can influence the cathodic reaction in CO_2 corrosion according to at least two possible scenarios. The first is HAc acting as a source of hydrogen ions through dissociation and the second is HAc being directly reduced on the metal surface. The present results as well as those recently presented by Sun et al. (2003) appear to support the former scenario while some of our subsequent studies at high pressure and temperature as well as the work of Garsany et al. (2002) seem to support the latter scenario. Furthermore, electrochemical models describing both scenarios were made and successfully fitted to the experimental data providing more evidence that it is very difficult to distinguish the reduction of hydrogen ions from direct HAc reduction at the electrode surface. This does not come as a surprise as a similar dilemma related to H_2CO_3 reduction defied a definitive answer since the mid seventies.

In the text below it will be assumed that HAc acts solely as a source of hydrogen ions and therefore compared to the electrochemical model of Nesic et al. (1996) only a slight modification to the hydrogen ion reduction equation, related to the calculation of the limiting current, needs to be made. Only one anodic reaction is assumed to be present, which is the dissolution of iron.

Hydrogen Ion Reduction

To find the effect of charge transfer and mass transfer on hydrogen ion reduction, the cathodic part of the rate equation is used (West 1964):

$$i_{(H^+)} = i_{0(H^+)}\left(\frac{[H^+]_s}{[H^+]_b}\exp\left(\frac{\alpha_c F}{RT}\eta\right)\right) \tag{1}$$

where $i_{0(H+)}$ is the exchange current density in A/m^2, $[H^+]_s$ and $[H^+]_b$ are the concentrations of hydrogen ions at the metal surface and bulk, respectively in mol/m^3, α_c is the symmetry factor, and η is the overpotential from the reversible potential in V. The overpotential is the difference between the applied potential and the reversible potential. The reversible potential for hydrogen reduction (E_{rev}) is found as:

$$E_{rev(H^+)} = -\frac{2.303RT}{F}pH - \frac{2.303RT}{2F}\log P_{H_2} \tag{2}$$

where P_{H2} is the partial pressure of hydrogen in atm. The partial pressure of hydrogen was assumed to be zero in the experiments. The surface hydrogen ion concentration can be found from the mass transfer equation:

$$i_{(H^+)} = k_m F([H^+]_b - [H^+]_s) \tag{3}$$

where k_m is the mass transfer coefficient of hydrogen in m/s. Substitution of Equation (3) into (1) and solving for $[H^+]_s$ yields the final current density vs voltage equation for H^+ reduction:

$$\frac{1}{i_{(H^+)}} = \frac{1}{i_{a(H^+)}} + \frac{1}{i^d_{\lim(H^+)}} \tag{4}$$

where $i_{a(H+)}$ is the activation current density in A/m^2 and $i^d_{lim(H+)}$ is the diffusion limiting current density in A/m^2. The activation current density is given by:

$$i_{a(H^+)} = i_{0(H^+)} \times 10^{-\frac{\eta}{b_c}} \tag{5}$$

where $i_{0(H+)}$ is the exchange current density in A/m^2 and b_c is the cathodic Tafel slope in V/dec. The temperature dependence of the cathodic Tafel slope is given by:

$$b_c = \frac{2.303RT}{\alpha_c F} \tag{6}$$

while the temperature dependence of the exchange current density is given by:

$$\frac{i_0}{i_o^{ref}} = e^{-\frac{\Delta H}{R}(\frac{1}{T}-\frac{1}{T_{ref}})} \tag{7}$$

where ΔH is the enthalpy of activation in kJ/mol and i_o^{ref} is the reference exchange current measured at some reference temperature, T_{ref}.

Limiting Current for H^+ reduction

The mass transfer limiting current density from Equation (4) is calculated by:

$$i^d_{\lim(H^+)} = k_m F[H^+]_b \tag{8}$$

where the mass transfer coefficient, k_m, is found from the rotating cylinder correlation (Eisenberg 1954):

$$Sh = \frac{k_m d}{D} = 0.0791 \times Re^{0.7} \times Sc^{0.356} \tag{9}$$

where d is the diameter of the electrode in m, D is the hydrogen diffusion coefficient in m^2/s, Re is the Reynolds number and Sc is the Schmidt number. The temperature dependence of the diffusion coefficient is given by:

$$D = D_{ref}\left(\frac{T}{T_{ref}}\right)\left(\frac{\mu_{ref}}{\mu}\right) \tag{10}$$

where D_{ref} is the diffusion coefficient at a reference temperature T_{ref}, μ is the viscosity in kg/(m s) and μ_{ref} is the viscosity at a reference temperature. At 20°C, the μ_{ref} of water is 1.002 kg/(m s) and the D_{ref} of hydrogen ion is 9.31×10^{-9} m^2/s (Atkins, 1982). The water density in kg/m^3 is found from:

$$\rho = 1152.3 - 0.5116T \tag{11}$$

while the water viscosity is given by:

$$\mu = \mu_{ref} \times 10^{\frac{1.3272(2-t)-0.001053(20-t)^2}{t+105}} \tag{12}$$

Limiting Current Arising from the Presence of HAc

Vetter (1976) proposed that limiting currents could result from chemical reactions if a slow chemical reaction precedes the hydrogen ion reduction reaction. He termed this limiting current a "chemical reaction" limiting current. He then derived equations to predict the chemical reaction limiting currents produced in stagnant weak acid solutions using HAc as the example. Nesic et al. (1995) expanded the equations to flowing systems using the example of carbonic acid as the weak acid. In order to predict the limiting currents in the case of flowing systems in the presence of HAc, Vetter's/Nesic's derivation will need to be re-derived with flow taken into account. The final equation to predict the reaction limiting current has the form:

$$i_{\lim(H^+)} = Fc_b\sqrt{Dk_r[Ac^-]}f \tag{13}$$

where k_r is the reaction rate constant from the dissociation reaction of HAc and *f* is defined as the flow factor, which is given:

$$f = \frac{1 + e^{-2\delta_m / \delta_r}}{1 - e^{-2\delta_m / \delta_r}} \tag{14}$$

where δ_r and δ_m are the reaction and mass transfer layer thicknesses, respectively, and are calculated from:

$$\delta_r = \sqrt{\frac{Dc_b}{v_0}} = \sqrt{\frac{Dc_b}{kc_b}} = \sqrt{\frac{D}{k_r[Ac^-]}} \tag{15}$$

$$\delta_m = \frac{D}{k_m} \tag{16}$$

where ν_0 is the rate of hydrogen production at equilibrium and D is the diffusivity of hydrogen ions in m^2/s.

The calculated reaction limiting currents are compared to the experimentally observed limiting currents in HAc solutions de-oxygenated using N_2 or CO_2 in Table 3. It is evident that the calculated reaction limiting currents are not in agreement and are even orders of magnitude larger than the measured values. This is proof that the limiting currents measured in the presence of HAc are not reaction rate controlled. It is worth noting that the flow factor *f*, in the presence of HAc, is equal to unity since the reaction layer thickness is typically two orders in magnitude smaller than the mass transfer boundary layer as the dissociation is very fast (Vetter 1976).

Since the HAc limiting currents are not chemical reaction limiting, they could be mass transfer limiting. The mass transfer limiting current density has the same form as the limiting current density for the hydrogen ion and is given by:

$$i^d_{\lim(HAc)} = k_m F[HAc]_b \tag{17}$$

where k_m is the HAc mass transfer coefficient in m/s and $[HAc]_b$ is the bulk concentration of HAc.

The calculated reaction limiting currents using Equation (17) are compared to the experimentally observed limiting currents in HAc solutions de-oxygenated using N_2 or CO_2 in Table 4. It is evident that the calculated limiting currents are similar in magnitude to the experimental values. In N_2 purged solutions, the measured and calculated limiting currents are in good agreement. The limiting currents measured in CO_2 purged solutions would be in better agreement with the calculated values if the contribution of hydrogen ions and carbonic acid to the limiting currents were taken into account (performed below).

As it has been assumed above that HAc acts solely as a source of hydrogen ions only, then it is not involved in a separate cathodic reaction at the metal surface and only increases the limiting current as previously discussed. Therefore, the limiting current for hydrogen ion reduction, must be corrected to account for HAc transport to the metal surface by modifying Equation (4):

$$\frac{1}{i_{(H^+)}} = \frac{1}{i_{a(H^+)}} + \frac{1}{i^d_{\lim(H^+)} + i^d_{\lim(HAc)}} \tag{18}$$

where the limiting current density for HAc is given by Equation (17).

Limiting Current Arising from the Presence of CO_2

Since carbonic acid is also a weak acid like HAc, it would be consistent to assume that it too, would only act as a source of hydrogen ions and add to the limiting current. With this modification, the Equation(18) now has the final form:

$$\frac{1}{i_{(H^+)}} = \frac{1}{i_{a(H^+)}} + \frac{1}{i^d_{\lim(H^+)} + i^d_{\lim(HAc)} + i^r_{\lim(H_2CO_3)}} \tag{19}$$

where $i^r_{\lim(H_2CO_3)}$ is found using the same derivation as used for HAc and is given by Nesic (1995):

$$i^r_{\lim(H_2CO_3)} = F[CO_2]_b \sqrt{D_{H_2CO_3} K_{hyd} k^f_{hyd}}\, f \tag{20}$$

where $[CO_2]_b$ is the bulk concentration of carbon dioxide in mol/m^3, K_{hyd} is the equilibrium constant for carbon dioxide hydration (assumed to be equal to 2.58x10^{-3} 1/s.), k^f_{hyd} is the rate of hydration of carbon dioxide in 1/s and f is the flow multiplier that includes the effect of the reaction diffusion layer on the limiting current. The bulk concentration of carbon dioxide can be found from:

$$[CO_2]_b = k^d_{CO_2} \times P_{CO_2} \tag{21}$$

where P_{CO2} is the partial pressure of CO_2 in bar and k^d_{CO2} is Henry's constant in mol/bar which is given by (Nesic 1996):

$$k^d_{CO_2} = \frac{14.5}{1.00258} \times 10^{-(2.27+5.65\times10^{-3} T_f - 8.06\times10^{-6} T_f^2 + 0.075 I)} \tag{22}$$

where T_f is the system temperature in Fahrenheit and I is the ionic strength. The forward reaction rate, k^f_{hyd} is found from (Oddo 1982)

$$k^f_{hyd} = 10^{5.71+0.0526 x T_C - 2.94 x 10^{-4} x T_C^2 + 7.91 x 10^{-7} x T_C^3} \tag{23}$$

where T_c is the system temperature in °C.

Water Reduction

Since the concentration of water is very large near the metal surface, no diffusion limiting current exists, so only the charge-transfer process is considered. The reversible potential and Tafel slope for water reduction was assumed to be the same as the hydrogen ion. The exchange current density at 20°C was taken as 3x10^{-5} A/m^2 and the enthalpy of activation as 30 kJ/mol (Nesic et al. 1996). The contribution of this reaction to the total cathodic current is very small at the corrosion potential.

The Anodic Dissolution of Iron

The dissolution of iron around the corrosion potential was assumed to be under activation control and hence pure Tafel behavior was assumed.

$$i_{(Fe)} = i_{0(Fe)} \times 10^{\frac{\eta}{b_a}} \tag{24}$$

From the experimental data, the Tafel slope was found to be 80 mV/dec at all concentrations of HAc, but 40 mV/dec was used when HAc was not present in solution. The reversible potential of X-65 steel was taken to be –0.488 V (Nesic et al. 1996) and the enthalpy of activation was found to be 50 kJ/mol.

Implementation of the Model

Once implemented the model requires as inputs the temperature, pH, HAc concentration, partial pressure of CO_2, rotating cylinder diameter, and rotational velocity so that the current density for each reaction is calculated. The corrosion potential then is found by solving the charge balance equation:

$$\sum i_a = \sum i_c \tag{25}$$

which here takes the simple form:

$$i_{(Fe)} = i_{(H^+)} + i_{(H_2O)} \tag{26}$$

Once the corrosion potential is known, a potentiodynamic sweep can be predicted by solving for the difference between the sum of the cathodic reactions from the anodic reactions. The corrosion current or rate is found from the anodic current at the corrosion potential.

DE WAARD CORROSION MODEL

de Waard Corrosion Model (1995)

de Waard and Milliams first reported a CO_2 corrosion model for wet gas pipelines in 1975. The model was based on experimental data (weight loss and LPR measurements) taken from glass cells and autoclaves. The model is considered to be a "worst case" model due to its conservative estimate for the corrosion rate. The model, through the years, has been revised (1991, 1993 and 1995) to take into account new parameters important to the corrosion process as experimental data became available. For example, in the 1991 model revision, the effect of higher pressures, protective film formation, high system pH, presence of hydrocarbons and water condensation were taken into account. All of the parameters are accounted for in the model through the use of factors which are multiplied by the "worst case" corrosion rate.

In 1995, the effect of liquid velocity, steel composition and microstructure were included in the model after new experimental data was performed. The "worst case" corrosion rate was found from the following equation:

$$\frac{1}{V_{corr}} = \frac{1}{V_r} + \frac{1}{V_m} \tag{27}$$

where V_{corr} is the corrosion rate in mm/yr, V_r is the reaction rate in mm/yr and V_m is the maximum mass transfer rate of the corrosive species expressed in mm/yr. The charge transfer reaction rate can be written as:

$$V_r = A\left[H_2CO_3\right]^n e^{-\frac{\Delta E}{RT}} \tag{28}$$

where A is a constant, n is the reaction order and ΔE is the energy of activation for the reaction. If the carbonic acid concentration is eliminated by using the concentration of dissolved carbon dioxide, then the equation has the form:

$$V_r = A'(pCO_2)^n e^{-\frac{\Delta E}{RT}} \tag{29}$$

where A' is a new constant that includes the Henry's equilibrium constant for CO_2 dissolution, which was approximated by an exponential function. de Waard et al. (1993, 1995) then took logarithms of both sides to obtain:

$$\log(V_r) = c_1 + \frac{c_2}{T} + c_3 \log(pCO_2) \tag{30}$$

In 1993, de Waard and Lotz separated the corrosion rate calculation into charge transfer and mass transfer components and, in order to find the effect of the system pH on the charge transfer reaction rate, de Waard and Lotz (1993) modified the equation to have the form:

$$\log(V_r) = c_1 + \frac{c_2}{T} + c_3 \log(pCO_2) + c_4(pH_{actual} - pH_{CO_2}) \tag{31}$$

where pH_{actual} is the actual system pH in the presence of cations such as Ca^{2+}, Fe^{2+}, Mg^{2+}, etc., pH_{CO2} is the pure pH of the system from CO_2 dissolution only and the c_1 to c_4 are constants. The pH of the system from CO_2 is found from:

$$pH_{CO_2} = 3.71 + 0.00417T - 0.5 \times \log(pCO_2) \tag{32}$$

where pCO_2 is the partial pressure of carbon dioxide in bar.

The mass transfer component of the corrosion rate was found from:

$$V_m = k_m[CO_2] \tag{33}$$

where k_m is found from a Sherwood correlation for straight pipes (Pickett 1974) having the form:

$$Sh = \frac{k_m d}{D} = 0.023 Re^{0.8} Sc^{0.3} \tag{34}$$

where D is the diffusivity of the corrosive species in m^2/s, d is the pipe diameter in m, Re is the Reynolds number and Sc is the Schmidt number. de Waard et al. (1995) then solved for the mass transfer coefficient and combined the temperature dependent terms into a single constant, c_5.

$$k_m = 0.023\left(\frac{p^{0.5}D^{0.5}}{u^{0.5}}\right)\left(\frac{v^{0.8}}{d^{0.2}}\right) = c_5\left(\frac{v^{0.8}}{d^{0.2}}\right) \tag{35}$$

Substitution of Equation (35) into Equation (33) and adding the Henry's constant for CO_2 dissolution into the constant c_5 yields:

$$V_m = c_5\left(\frac{v^{0.8}}{d^{0.2}}\right)[pCO_2] \tag{36}$$

The constant which, until now, includes only temperature dependent terms (density, viscosity, etc.) was then used in conjunction with Equation (33) to fit the experimental data.

The two equations after fitting to the experimental data for normalized steels have the form:

$$\log(V_r) = 4.84 + \frac{1119}{T} + 0.58 \times \log(pCO_2) - 0.34(pH_{actual} - pH_{CO_2}) \tag{37}$$

$$V_m = 2.8\left(\frac{v^{0.8}}{d^{0.2}}\right)[pCO_2] \tag{38}$$

An Extension of the de Waard Model to Account for the Presence of HAc

A slight modification to the de Waard et al. model is needed to account for the presence of HAc. In Equation (27), the mass transfer term, V_m, includes only the transport of one corrosive species, carbonic acid, as shown by Equation (33). Equation 33 can be modified to account for the additional transport of HAc to the metal surface using:

$$V_{m(HAc)} = k_m[HAc] \tag{39}$$

where $V_{m(HAc)}$ is the mass transfer term for HAc in mm/yr, k_m is the mass transfer rate of HAc and $[HAc]$ is the bulk concentration of HAc. The mass transfer rate of HAc can be found by using Equation (9) with an appropriate expression for the diffusivity for HAc, such as Equation (10), when $D_{ref} = 1.24\text{x}10^{-9}$ m^2/s at 25°C (Perry 1984). The de Waard et al. model now has the final form:

$$\frac{1}{V_{corr}} = \frac{1}{V_r} + \frac{1}{V_{m_{(H2CO3)}} + V_{m_{(HAc)}}} \tag{40}$$

where $V_{m(H2CO3)}$ is the mass transfer rate of carbonic acid found from Equation (38). The constants in Equations (37) and (38), which were used to fit the original experimental data have not been changed with the modification to account for HAc.

ELECTROCHEMICAL MODEL VERSUS THE EXPERIMENTAL POTENTIODYNAMIC SWEEPS

The electrochemical model will be compared to the electrochemical data, which have been previously reported, by Sun et al. (2003). A predicted potentiodynamic sweep, shown in Figure 7, has been broken down according to the three individual sources of hydrogen ions, (transport of hydrogen ions from the bulk, and transport and dissociation of both carbonic acid and HAc) to show the effect of various contributions. It is clear that under these conditions HAc is the major source of hydrogen ions. Also shown in Figure 7 is the sum of the cathodic currents (total cathodic). This figure will serve as a template for subsequent comparison of the model and the experimental results. It is worth noting that the potentiodynamic sweeps, both experimental and those predicted by the model, have been moved from the corrosion potential due to the proprietary nature of some of the electrochemical constants in the model.

The Effect of HAc Concentration in CO_2 Solutions

The comparison between the electrochemical model and the experimental results for solutions purged by CO_2 are shown in Figures 8-11. It is evident that the model is in good agreement with the experimental data at all concentrations of HAc studied. The model predicts both the charge transfer and limiting current regions of the cathodic potentiodynamic sweeps very well. The anodic reaction is also predicted very well until pre-passivation of the metal surface occurs at higher anodic overpotentials.

The Effect of Rotational Velocity

The effect of rotational velocity manifests itself through increased transport of species and particularly HAc to the metal surface. The experimental and predicted potentiodynamic sweeps were found to be in very good agreement at all velocities. Only the minimum (500 rpm) and maximum (4000 rpm) velocities are compared here with the model and are shown in Figures 12 and 13.

The Effect of Temperature

The effect of temperature is shown in Figures 14-16. It is evident that the experimental and predicted potentiodynamic sweeps are in good agreement.

ELECTROCHEMICAL AND DE WAARD MODELS FOR CORROSION RATE PREDICTION VERSUS THE EXPERIMENTS

In order to compare the modified de Waard model (here called the George-de Waard-Nesic or GDN model), with the experimental data obtained by using a RCE, the equivalence between the two flow geometries must be found first. This equivalence can be achieved on the basis of equal mass transfer coefficients between the two systems. The mass transfer coefficient of hydrogen in a RCE was calculated from the Eisenberg correlation, Equation (9). For pipe flow, the Berger and Hau (1977) correlation is most appropriate.

$$Sh_p = \frac{k_m d_p}{D} = 0.0165 \times Re_p^{0.86} \times Sc^{0.33} \tag{41}$$

The RCE mass transfer coefficient for hydrogen ions is calculated from the Eisenberg correlation, and then used in the Berger and Hau correlation to solve for the flow velocity in the Reynolds number term. A pipe diameter must also be used and was taken as 0.1 m in the comparisons made below (although the effect is not large).

The comparison between the LPR, WL and the electrochemical and GDN models at 22°C is shown in Figure 17. At low concentrations of HAc (up to 100 ppm), the agreement between the experimental data and the electrochemical model is very good. Above 100 ppm, the electrochemical model does not agree with the experimental data. It is evident that the GDN model over predicts the corrosion rate at all concentrations of HAc.

The comparison between the LPR, WL and the electrochemical and GDN models at 40°C is shown in Figure 18. At 0 ppm HAc, the electrochemical model is in slightly better agreement with the experimental data when compared to the GDN model. At low concentrations of HAc (up to 100 ppm) the electrochemical and GDN model predict very similar corrosion rates, which agree well with the experimental data. However, the two models diverge in their predicted values at 1000 ppm HAc and the GDN model is in better agreement with the experimental data.

The comparison between the LPR, WL and the electrochemical and GDN models at 60°C is shown in Figure 19. At 0 ppm HAc, the electrochemical model is slightly more conservative than the experimental data indicates, while the GDN model under predicts the experimental data. At 10 ppm HAc, the GDN model again under predicts the corrosion rate while the electrochemical model agrees well with the experimental data. At 100 ppm HAc, the electrochemical model is too conservative in the corrosion rate predicted while the GDN model is in very good agreement with the experimental values. At high concentrations of HAc (1000 ppm) the electrochemical model is in very good agreement with the experimental data while the GDN model under predicts the corrosion rate.

CONCLUSIONS

- Weight loss and LPR measurements were successfully used to confirm the effect of HAc on CO_2 corrosion previously identified by using potentiodynamic sweeps.
- A new electrochemical model was built that includes the effect of HAc on cathodic reactions and did well in describing the electrochemical behavior as measured by using the potentiodynamic sweeps.
- A modification to the de Waard corrosion model (GDN model) has been made to account for the presence of HAc.
- Both the electrochemical model as well as the GDN model were in reasonable agreement with the experimental corrosion rates, measured by using LPR and weight loss.

ACKNOLDGEMENTS

The authors would like to acknowledge the contribution of the consortium of companies whose continuous financial support and technical guidance led to the development of the published work. They are BP, ConocoPhillips, ENI, Petrobras, Saudi Aramco, Shell, Total, Champion Technologies, Clariant, MI Technologies and Nalco. The Institute for Corrosion would also like to thank Dr. deWaard for his efforts in the development of this work.

REFERENCES

1. F.P. Berger, K. F.F-L Hau, *Int J Heat Mass Transfer*, Vol 20, 1977, p 1185.
2. J-L. Crolet, N. Thevenot, and A. Dugstad, "Role of Free Acetic Acid on the CO_2 Corrosion of Steels," CORROSION/1999, Paper No. 24, (Houston, TX: NACE International, 1999).
3. C. de Waard, D.E. Milliams, "Carbonic Acid Corrosion of Steel", *Corrosion*, Vol 31, No 5, 1975, p 175.
4. C. de Waard, U. Lotz, and D.E. Milliams, "Prediction Model for CO_2 Corrosion Engineering in Wet Gas Pipelines", *Corrosion*, Vol 47, No 12, 1991, p 976.
5. C. de Waard, U. Lotz, "Prediction of CO_2 Corrosion in Carbon Steel", CORROSION/1993, Paper No. 69, (Houston, TX: NACE International 1993).
6. C. de Waard, U. Lotz, A. Dugstad, "Influence of Liquid Flow Velocity on CO_2 Corrosion: A Semi-Empirical Model", CORROSION/1995, Paper No. 128, (Houston, TX: NACE International, 1995).
7. M. Eisenberg, C.W. Tobias, C.R. Wilke, *J Electrochemical Society*, Vol 101, 1954, p 306.
8. Y. Garsany, D. Pletcher, B. Hedges, "The Role of Acetate in CO_2 Corrosion of Carbon Steel: Has the Chemistry Been Forgotten?" CORROSION/2002, Paper No. 2273, (Denver, CO: NACE International, 2002).
9. Y.M. Gunaltun, D. Larrey, "Correlation of Cases of Top of Line Corrosion With Calculated Water Condensation Rates", CORROSION/2000, Paper No. 71, (Houston, TX: NACE International 2000).
10. B. Hedges, L. McVeigh, "The Role of Acetate in CO_2 Corrosion: The Double Whammy" CORROSION/1999, Paper no. 21, (Houston TX: NACE International 1999).
11. S. Nesic, B.F.M. Pots, J. Postlethwaite, N. Thevenot, "Superposition of Diffusion and Chemical Reaction Controlled Limiting Currents – Application to CO_2 Corrosion," *J Corrosion Science and Engineering*, Vol 1, Paper 3, 1995.
12. S. Nesic, G.T. Solvi, J. Enerhaug, "Comparison of the Rotating Cylinder and Pipe Flow Tests for Flow-Sensitive Carbon Dioxide Corrosion," *Corrosion*, Vol 51, No. 10, 1995, p 773.
13. S. Nesic, J. Postlethwaite, S. Olsen, "An Electrochemical Model for Prediction Of Corrosion of Mild Steel in Aqueous Carbon Dioxide Solutions," *Corrosion*, Vol 52, No 4, April 1996, p 280.
14. J.E.Oddo, M.B. Tomsom, "Simplified Calculation of $CaCO_3$ Saturation at High Temperature and Pressures in Brine Solutions," SPE of AIME, 1982, p 1583.
15. Pickett, *Electrochimica Acta*, Vol 19, 1974, p 875.
16. Y. Sun, K. George, S. Nesic, "The Effect of Cl- and Acetic Acid on Localized CO2 Corrosion in Wet Gas Flow", CORROSION/2003, Paper No. 3327, (Houston, TX: NACE International 2003).
17. J. M. West, Electrodeposition and Corrosion Processes, Van Nostrand, 1964, p 36.
18. K.J. Vetter, Electrochemical Kinetics – Theoretical and Experimental Aspects, New York, Academic Press, 1976.

TABLE 1. CHEMICAL COMPOSITION OF 5LX65 USED IN RCE (wt%)

Cr	Mo	S	V	Si	C	Fe	Ni	Mn	P
0.011	0.103	0.004	0.055	0.240	0.150	Balance	0.020	1.340	0.011

TABLE 2. TEST MATRIX FOR THE EXPERIMENTAL WORK

Liquid Phase	3 % NaCl, Simulated Brine
Gases used for De-oxygenation	Carbon Dioxide
HAc Concentration	0 – 1000 ppm
Temperature	22-60°C
pH	4.00
Rotational Velocity	1000 rpm
Material	X65
Measurement Techniques	LPR, EIS, Potentiodynamic Sweeps, Weight loss

TABLE 3. CHEMICAL COMPONENTS OF THE SIMULATED BRINE SOLUTION

Species	Wt %
NaCl	58.490
$MgCl_2*H_2O$	26.460
$NaSO_4$	9.750
$CaCl_2$	2.785
KCl	1.645
$NaHCO_3$	0.477
KBr	0.238
H_2BO_4	0.071
$SrCl_2*6H_2O$	0.095
NaF	0.007

TABLE 3. COMPARISION BETWENN THE EXPERIMENTAL AND CALCULATED LIMITING CURRENTS IN SOLUTIONS DE-OXYGENATED USING CO_2 AND N_2.

Conc of HAc (ppm)	Experimental i_{lim} in N_2	Experimental i_{lim} in CO_2	Calculated by Eqn 13 (A/m^2)	Calculated by Eqn 17 (A/m^2)
0	2	3	--	--
10	--	4	578	1
100	6	12	1830	7
1000	47	57	5780	69
5000	--	94	12900	347

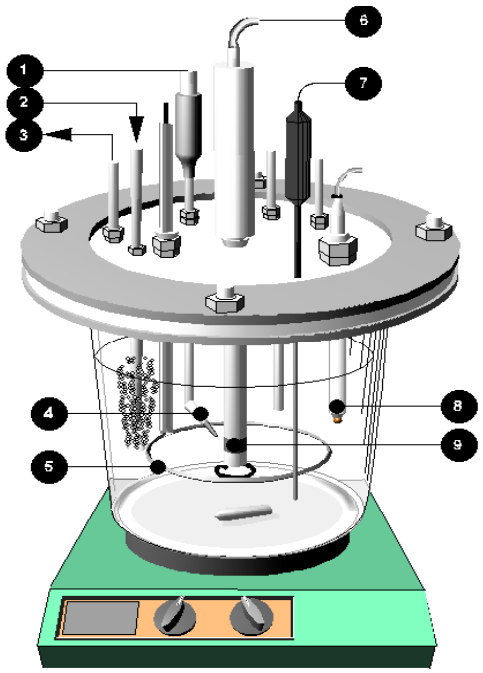

Figure 1. Schematic of the test cell. 1-reference electrode, 2-gas in, 3-gas out, 4-Luggin capillary, 5-Pt counter electrode, 6-rotator, 7-temperature feed-back probe, 8-pH probe, 9-working electrode.

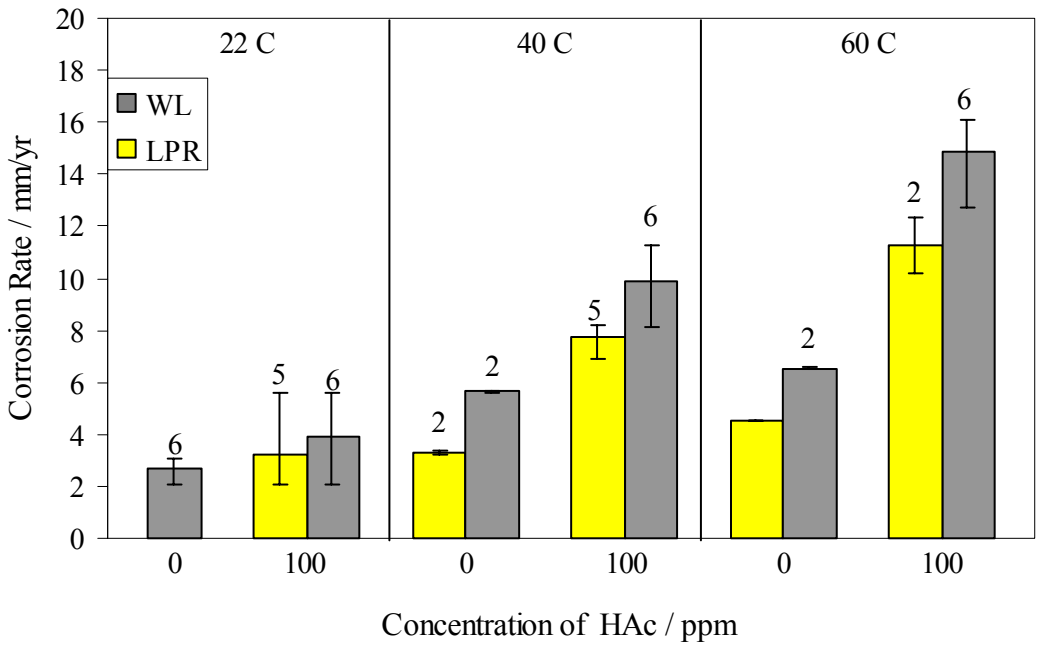

Figure 2. The effect of HAc and temperature on the corrosion rate of X-65 steel in bubbling CO_2 solutions containing 100 ppm HAc (pH 4, 1000 rpm). Error bars represent the maximum and minimum experimental values. The number of experiments is also indicated.

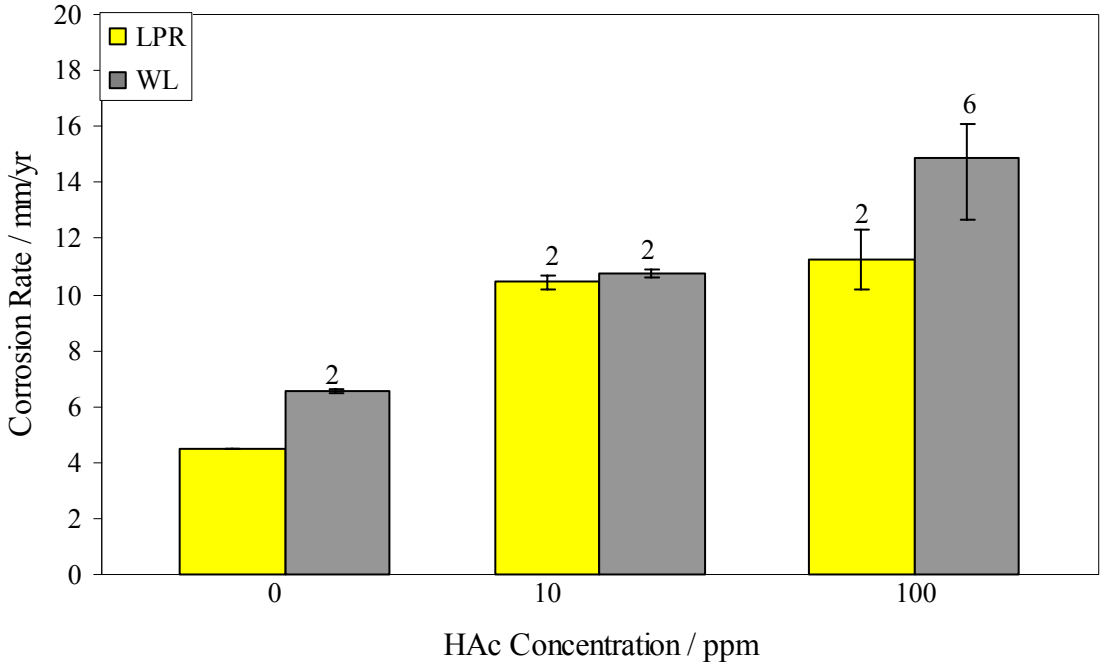

Figure 3. The effect of HAc concentration on the corrosion rate of X-65 steel in bubbling CO_2 solutions (60°C, pH 4, 1000 rpm). Error bars represent the maximum and minimum experimental values. The number of experiments is also indicated.

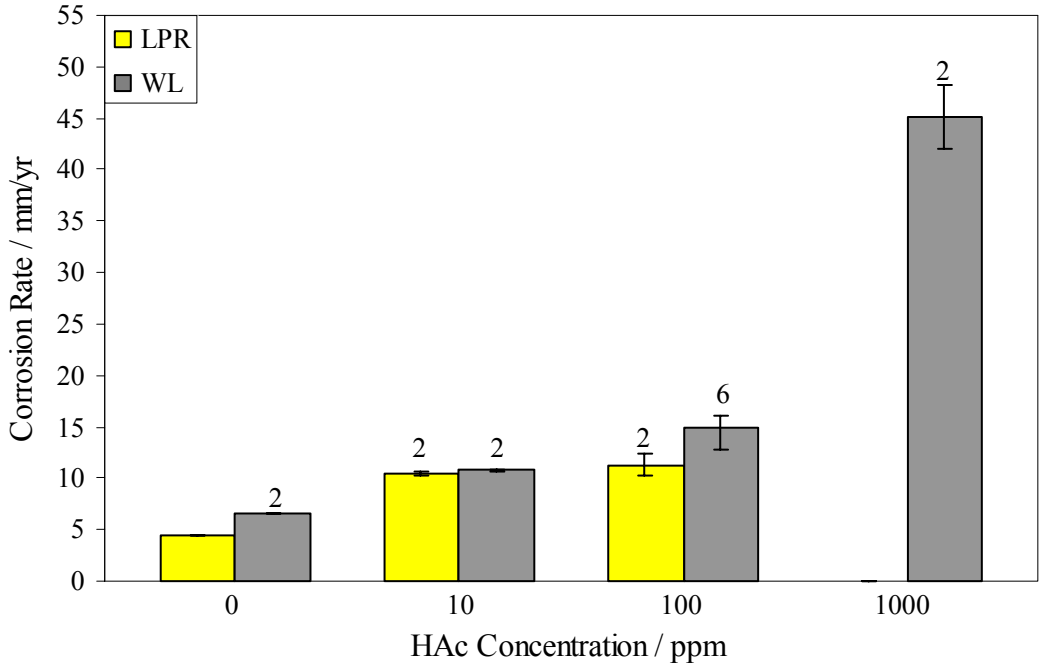

Figure 4. The effect of HAc on the corrosion rate of X-65 steel in bubbling CO_2 solutions (60°C, pH 4, 1000 rpm). Error bars represent the maximum and minimum experimental values. The number of experiments is also indicated.

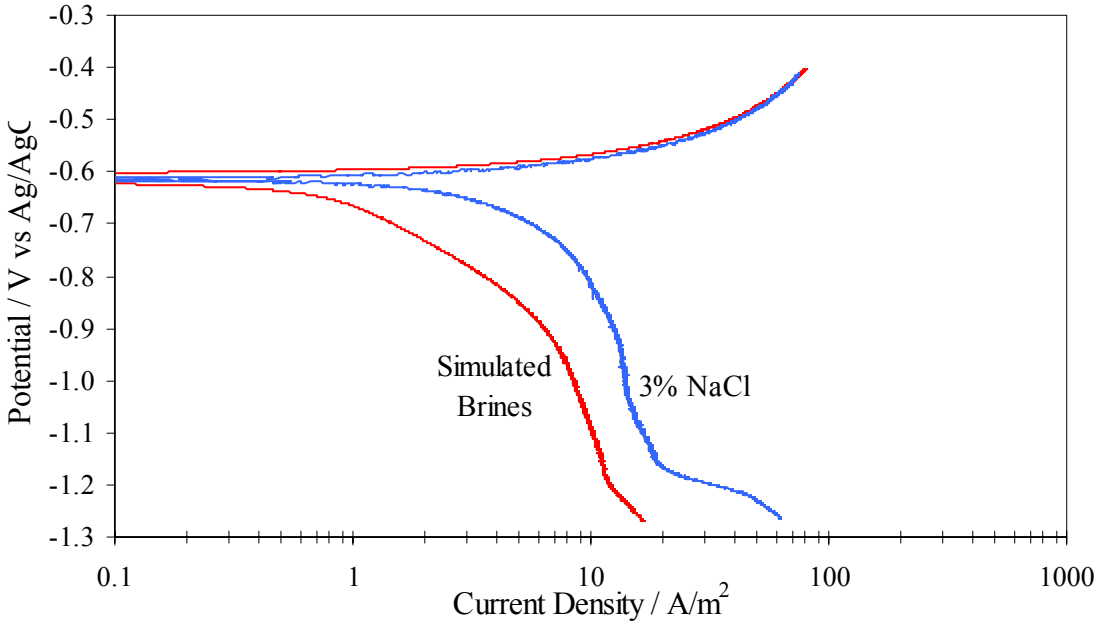

Figure 5. Potentiodynamic sweeps in 3% NaCl and simulated brine solutions containing 100 ppm HAc (22°C, pH 4, 1000 rpm)

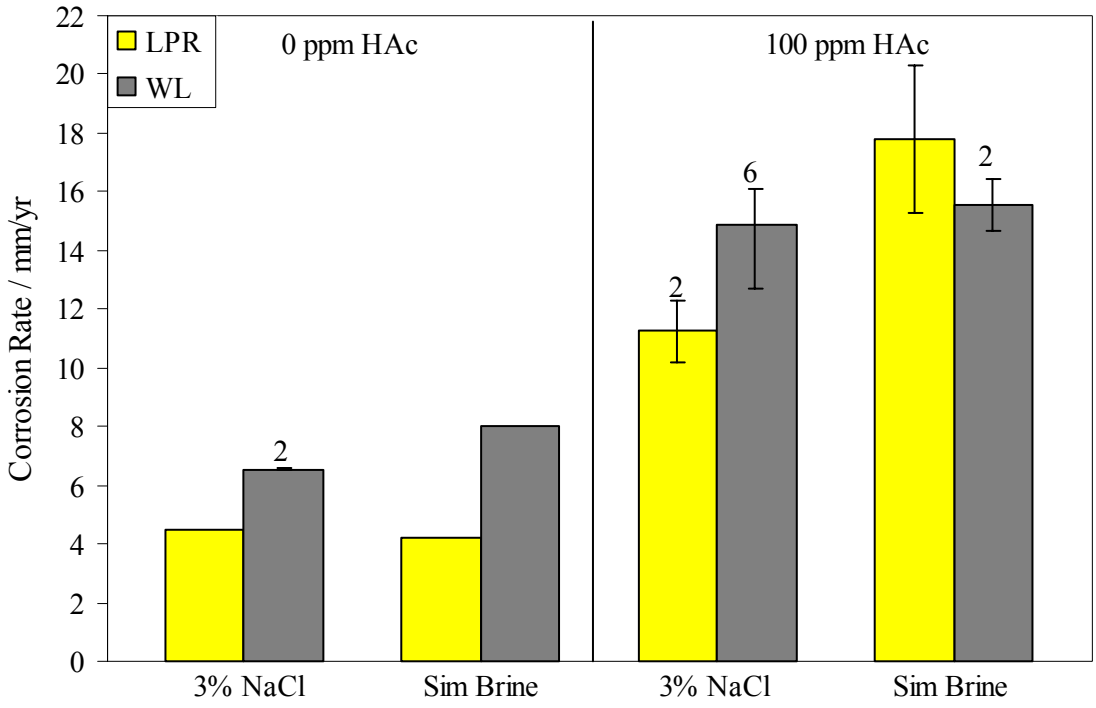

Figure 6. The effect of simulated brines and HAc concentration on the corrosion rate of X-65 steel in bubbling CO_2 solutions (60°C, pH 4, 1000 rpm). Error bars represent the maximum and minimum experimental values. The number of experiments is also indicated.

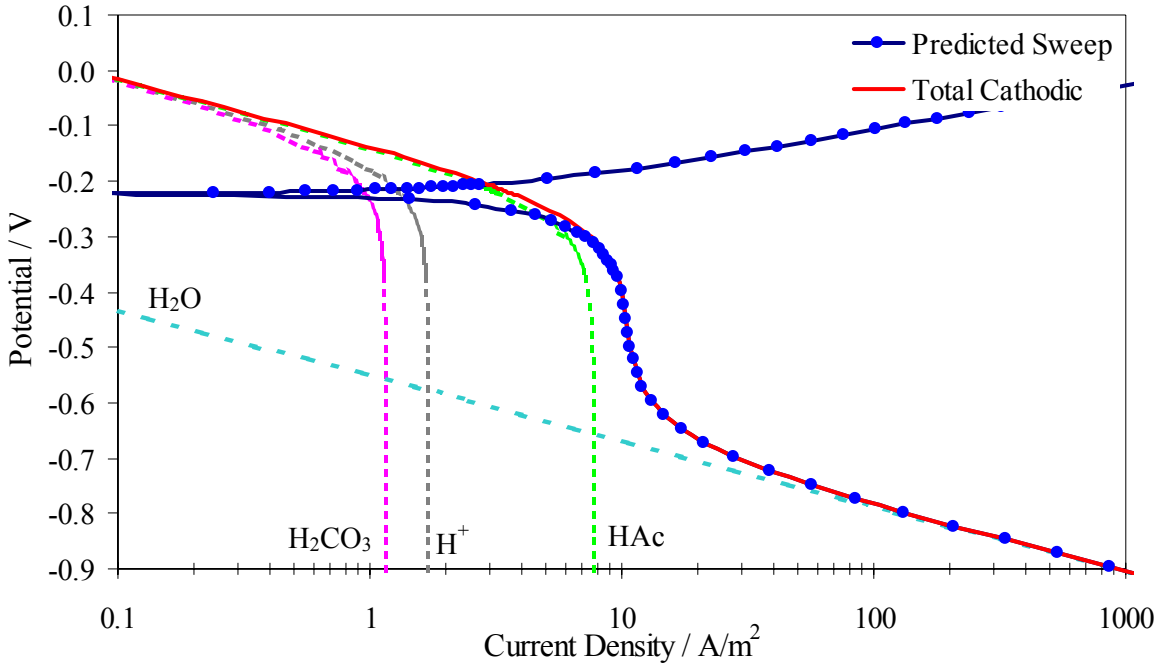

Figure 7. The electrochemical reactions in bubbling CO_2 solutions containing 100 ppm HAc (22°C, pH 4, 1000 rpm).

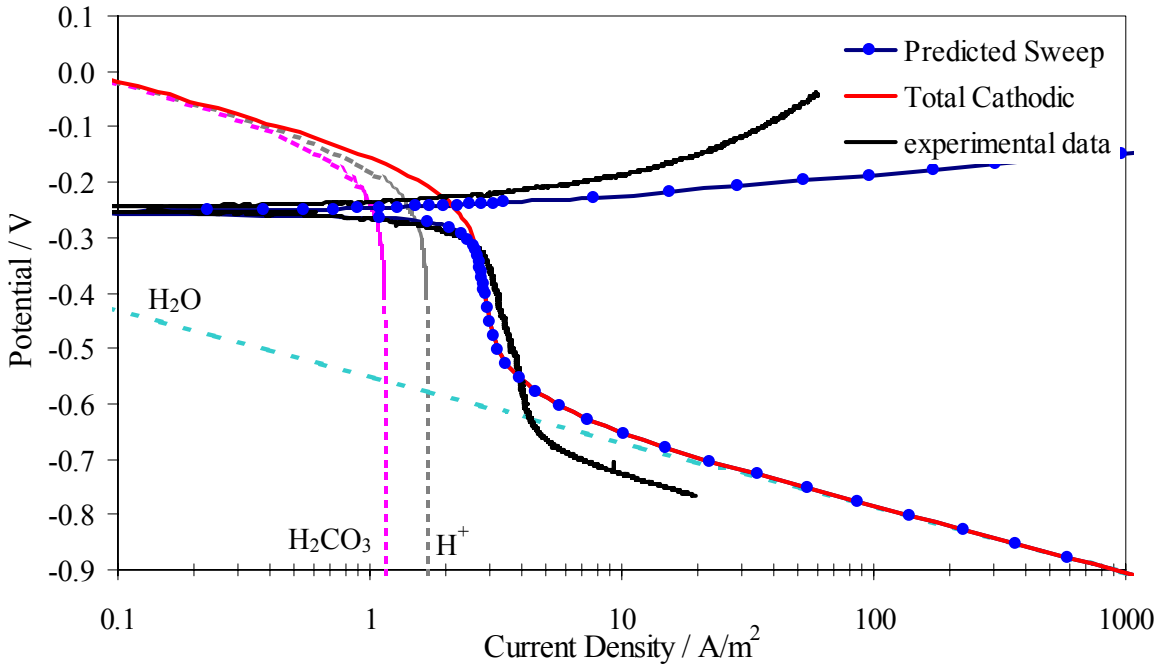

Figure 8. Comparison between the electrochemical model and experimental data in bubbling CO_2 solutions containing 0 ppm HAc (22°C, pH 4, 1000 rpm).

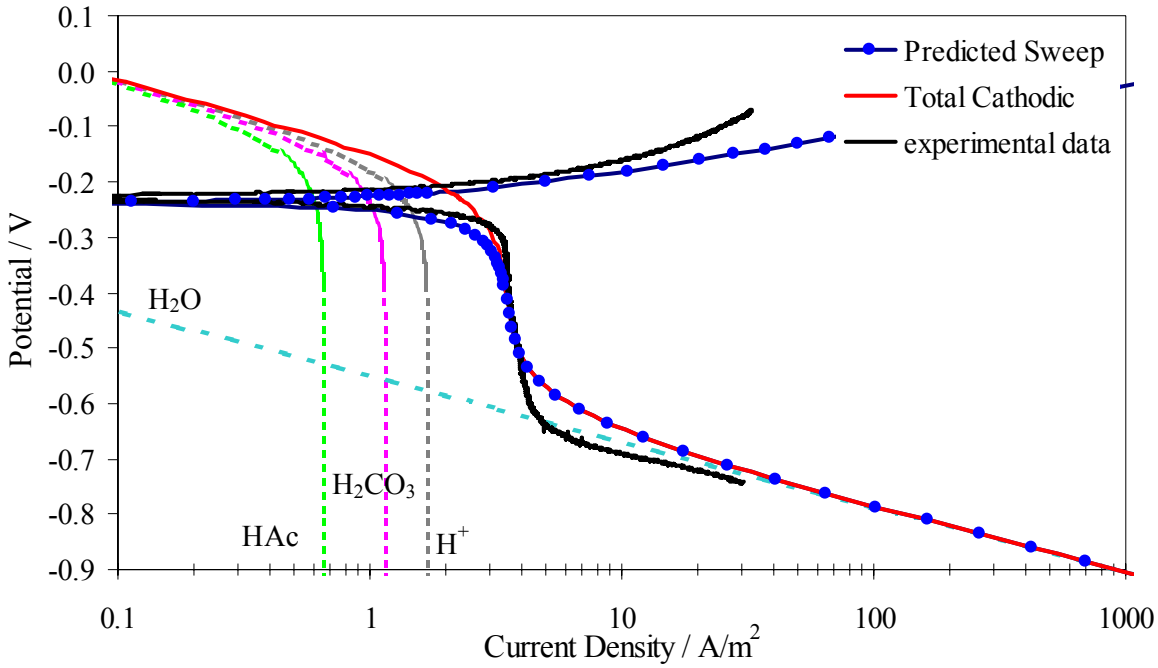

Figure 9. Comparison between the electrochemical model and experimental data in bubbling CO_2 solutions containing 10 ppm HAc (22°C, pH 4, 1000 rpm).

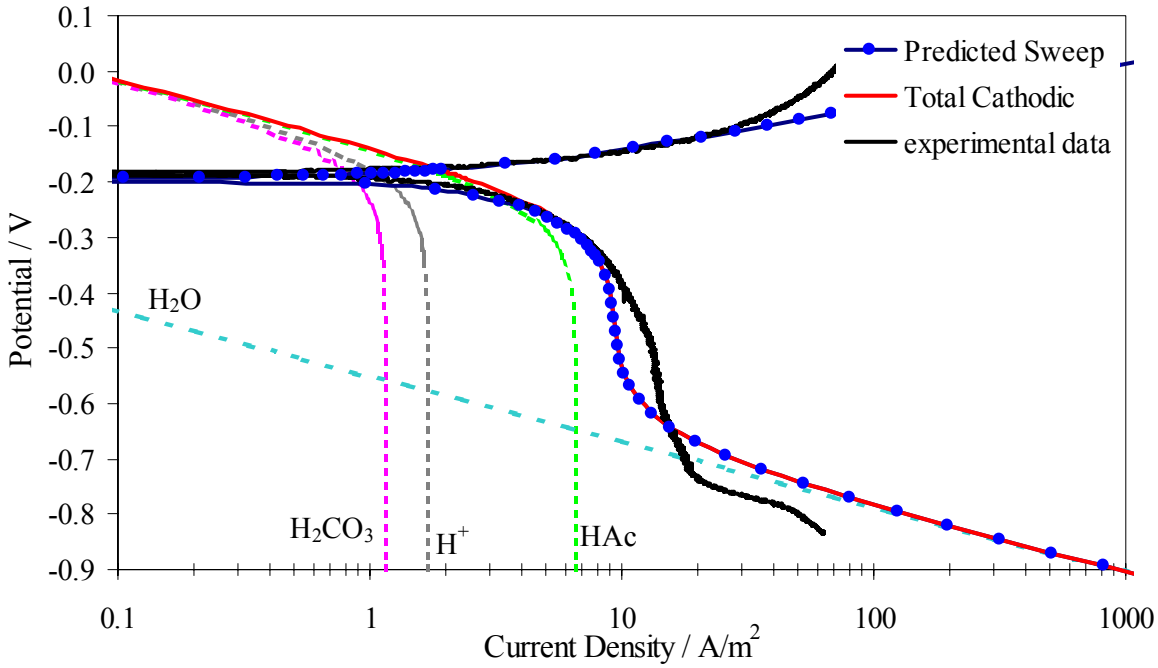

Figure 10. Comparison between the electrochemical model and experimental data in bubbling CO_2 solutions containing 100 ppm HAc (22°C, pH 4, 1000 rpm).

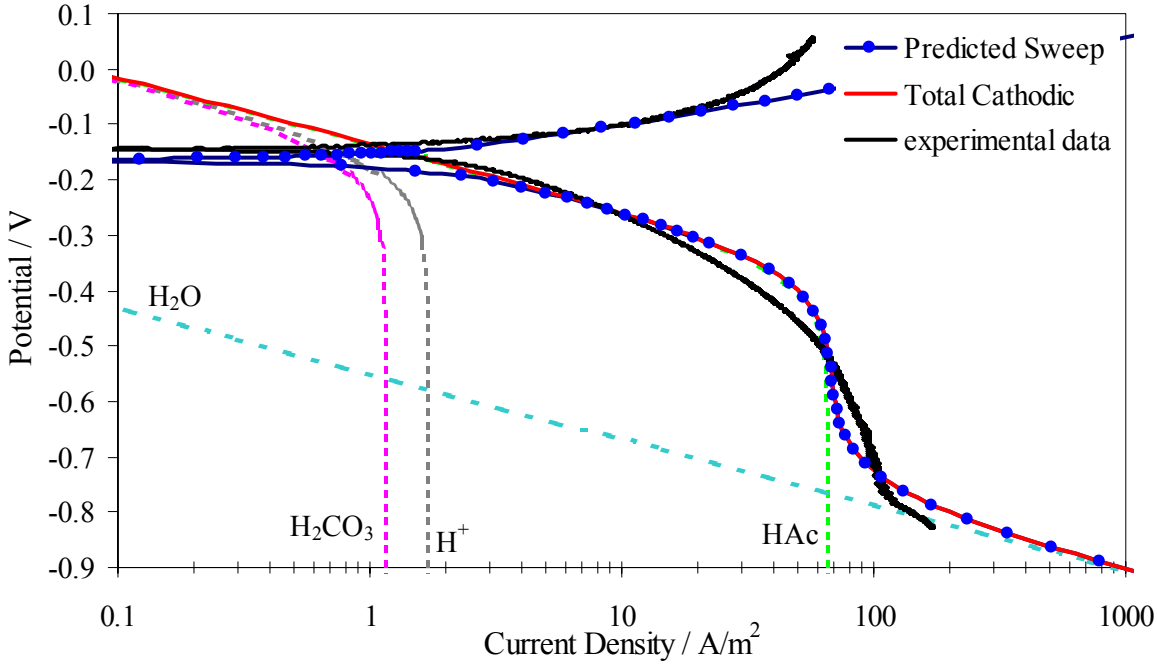

Figure 11. Comparison between the electrochemical model and experimental data in bubbling CO_2 solutions containing 1000 ppm HAc (22°C, pH 4, 1000 rpm).

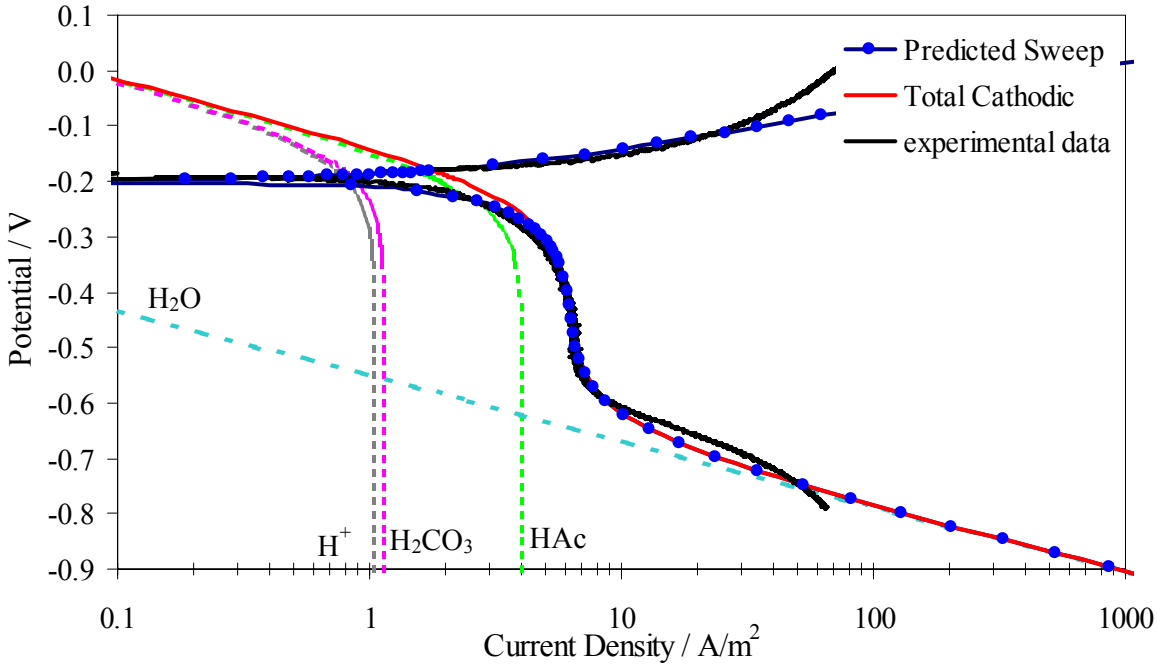

Figure 12. Comparison between the electrochemical model and experimental data in bubbling CO_2 solutions at 500 rpm (22°C, 100 ppm HAc, pH 4).

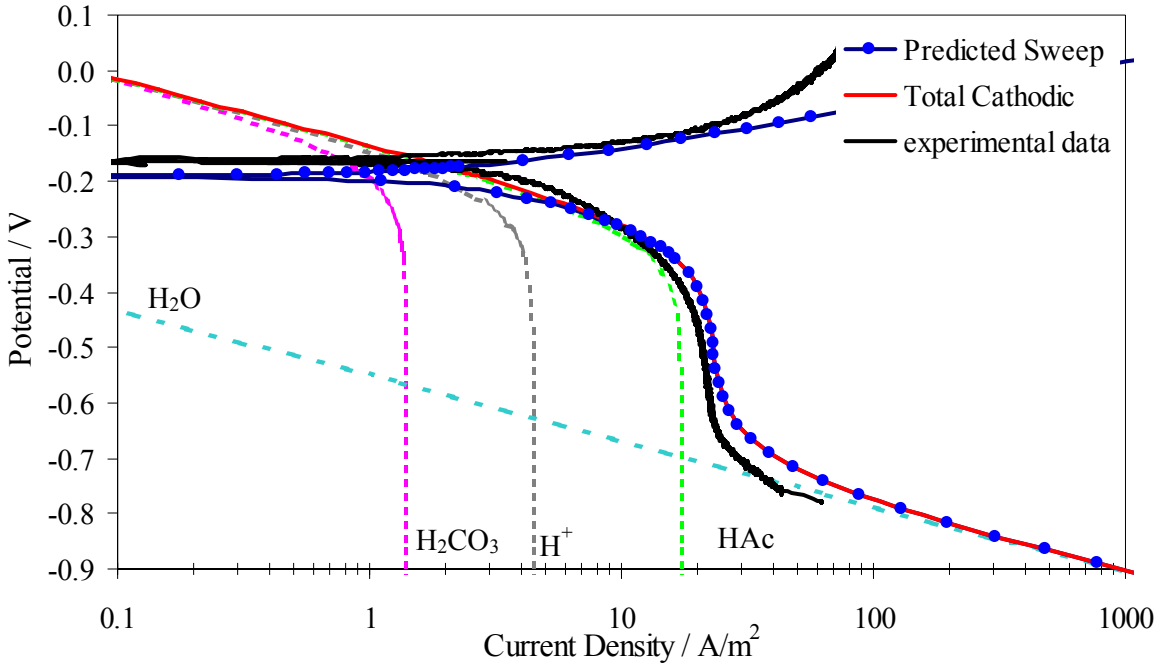

Figure 13. Comparison between the electrochemical model and experimental data in bubbling CO_2 solutions at 4000 rpm (22°C, 100 ppm HAc, pH 4).

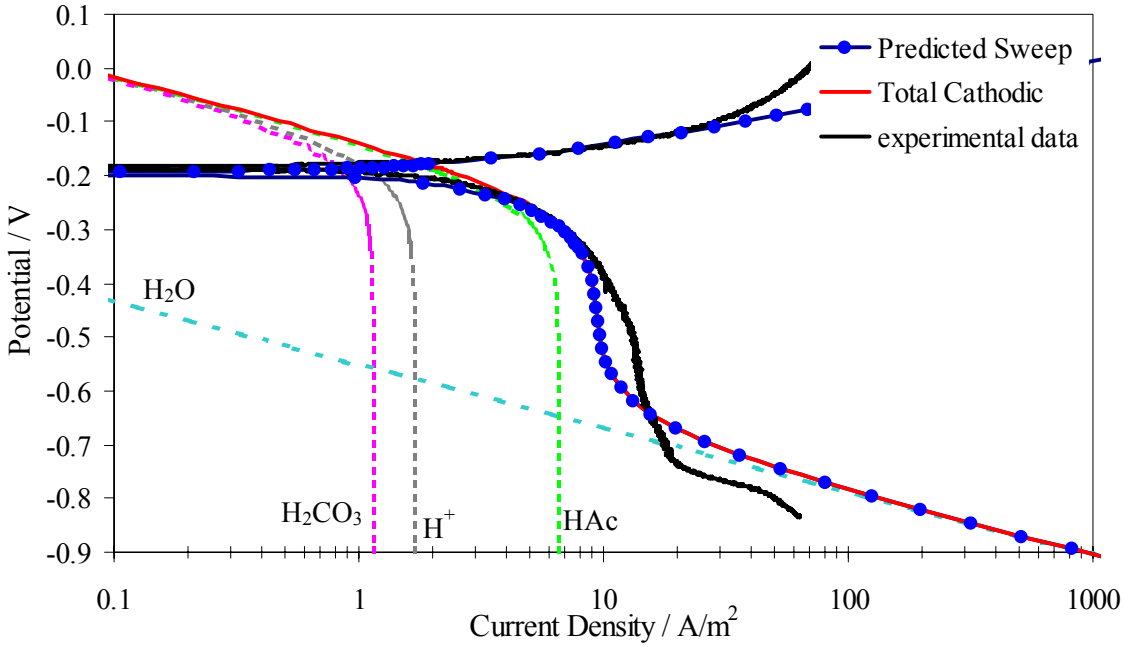

Figure 14. Comparison between the electrochemical model and experimental data in bubbling CO_2 solutions at 22°C (100 ppm HAc, pH 4, 1000 rpm).

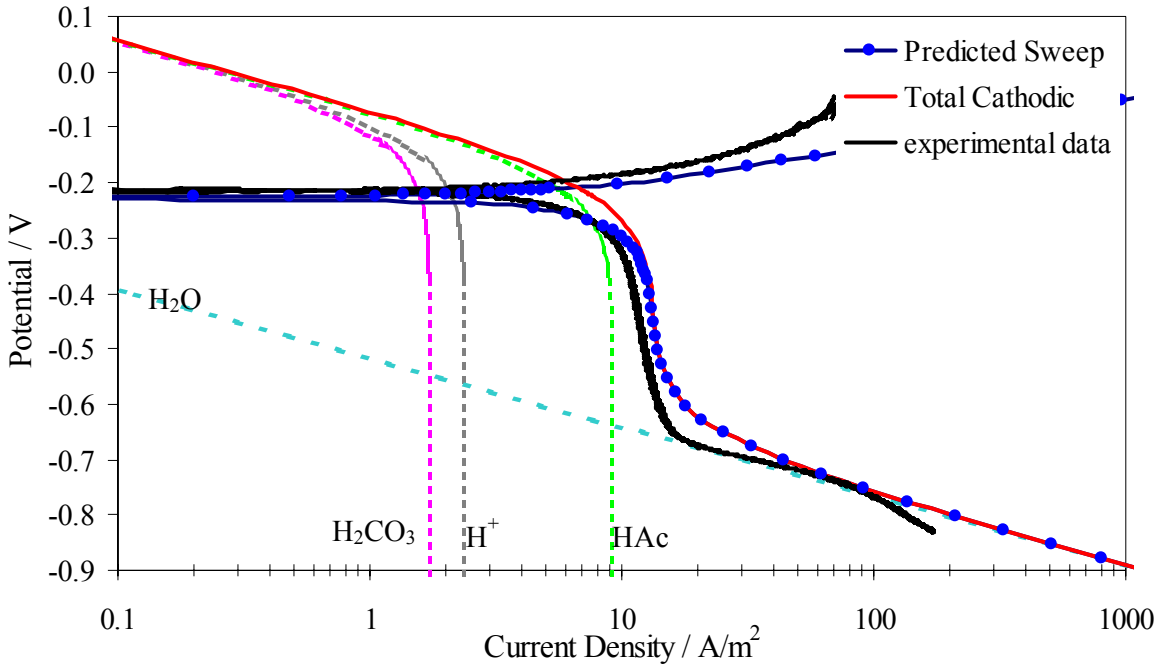

Figure 15. Comparison between the electrochemical model and experimental data in bubbling CO_2 solutions at 40°C (100 ppm HAc, pH 4, 1000 rpm).

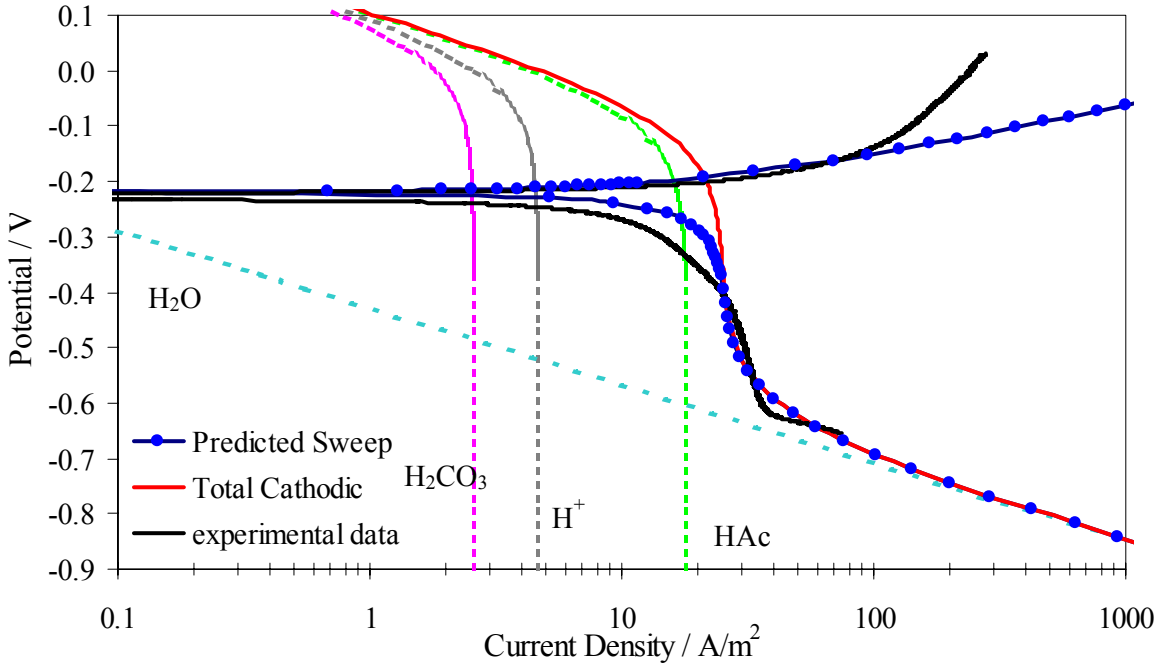

Figure 16. Comparison between the electrochemical model and experimental data in bubbling CO_2 solutions at 80°C (100 ppm HAc, pH 4, 1000 rpm).

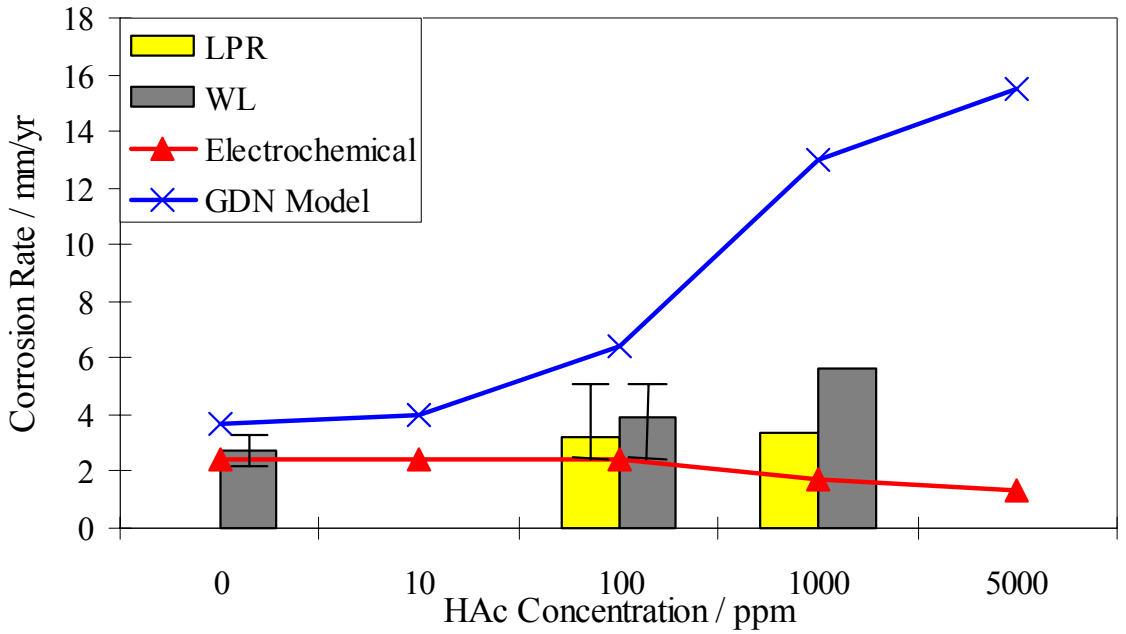

Figure 17. Comparison between the experimental data and electrochemical and GDN models at 22°C (0-5000 ppm HAc, pH 4, 1000 rpm). Error bars represent the maximum and minimum experimental values.

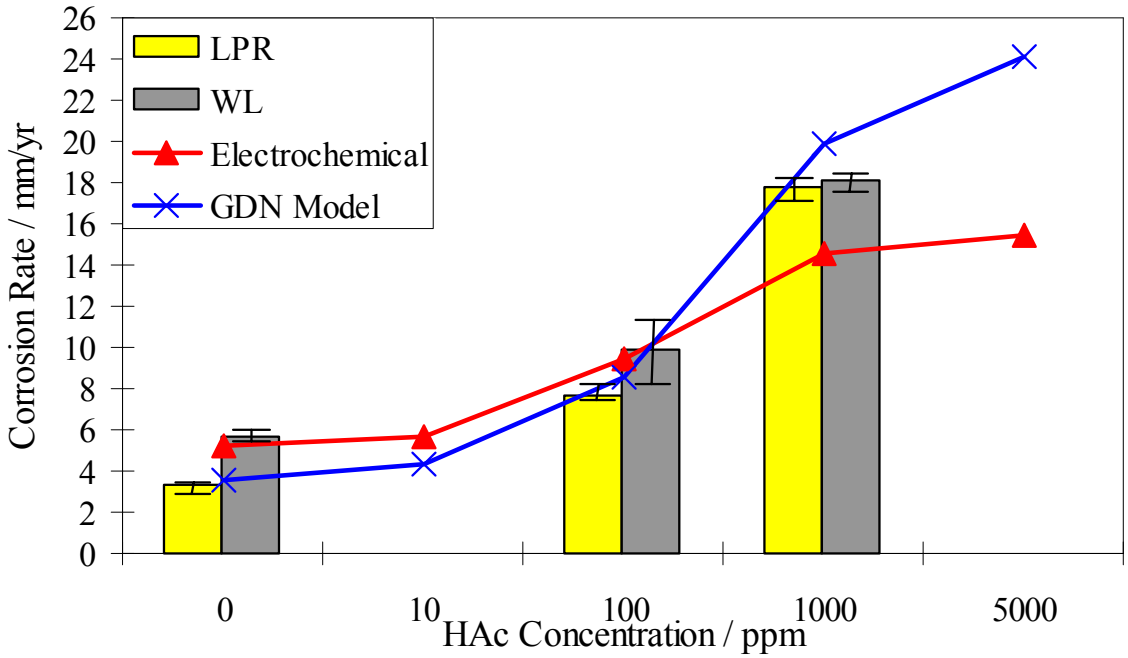

Figure 18. Comparison between the experimental data and electrochemical and GDN models at 40°C (0-5000 ppm HAc, pH 4, 1000 rpm). Error bars represent the maximum and minimum experimental values.

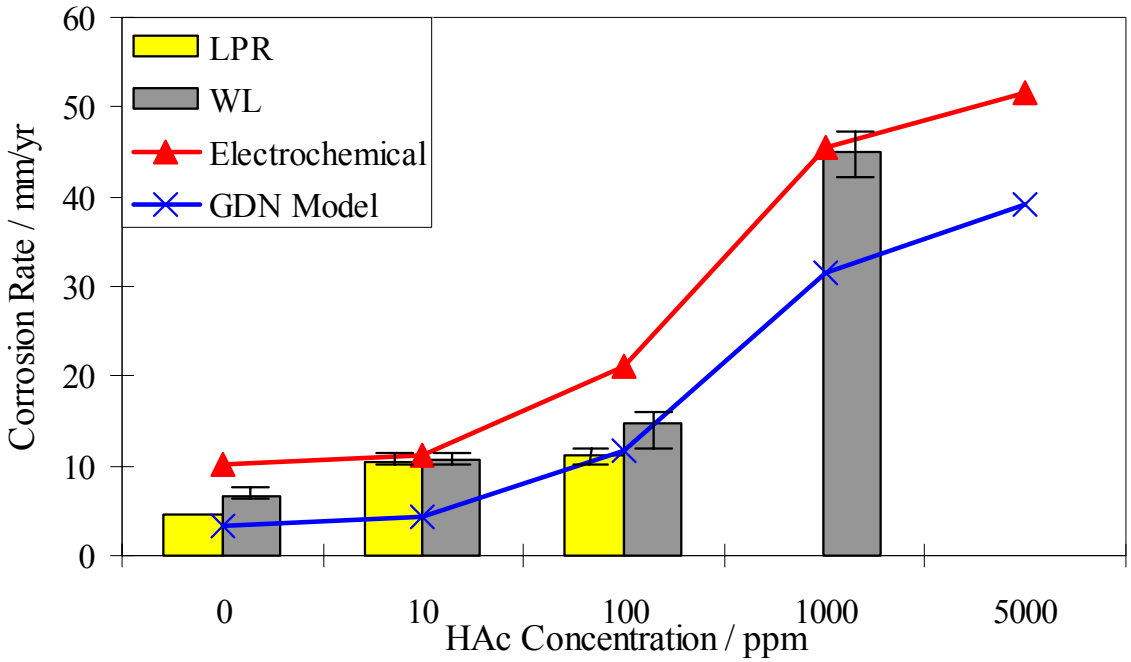

Figure 19. Comparison between the experimental data and electrochemical and GDN models at 60°C (0-5000 ppm HAc, pH 4, 1000 rpm). Error bars represent the maximum and minimum experimental values.